Group delay dispersion monitoring for computational manufacturing of dispersive mirrors

XIAOCHUAN JI,[1,2] JIANGLIN DAI,[1,2] JINLONG ZHANG,[1,2,*] HONGFEI JIAO,[1,2] MARCO JUPÉ,[3,4] DETLEV RISTAU,[3,4] XINBIN CHENG,[1,2] AND ZHANSHAN WANG[1,2]

[1]*MOE Key Laboratory of Advanced Micro-Structured Materials, Tongji University, Shanghai, 200092, China*
[2]*Institute of Precision Optical Engineering, School of Physics Science and Engineering, Tongji University, Shanghai, 200092, China*
[3]*Laser Zentrum Hannover e.V., Laser Components Department, Hollerithallee 8, 30419, Hanover, Germany*
[4]*Leibniz Universität Hannover, Institut für Quantenoptik, Welfengarten 1, 30167 Hanover, Germany*
[*]*jinlong@tongji.edu.cn*

Abstract: We present a computational manufacturing program for monitoring group delay dispersion (GDD). Two kinds of dispersive mirrors computational manufactured by GDD, broadband, and time monitoring simulator are compared. The results revealed the particular advantages of GDD monitoring in dispersive mirror deposition simulations. The self-compensation effect of GDD monitoring is discussed. GDD monitoring can improve the precision of layer termination techniques, it may become a possible approach to manufacture other optical coatings.

1. Introduction

During the last decades, ultrafast laser systems offer potential applications in advanced scientific fields such as frequency comb spectroscopy, ultra-precise material processing and medical diagnostics [1,2]. In 1994, Szipöcs et al. [3] first invented dispersive mirrors, which have great potential in phase modulation and have attracted many scientists. Owing to the success of dispersive mirrors, ultrafast optics technology continues moving towards shorter durations and higher intensities [4]. Multilayer dielectric dispersive mirrors are popular in femtosecond and attosecond physics because of their accurate control of group delay dispersion (GDD) and spectral integration ability [5,6]. For example, precise broadband GDD control allows the generation of laser pulses with durations <3fs from a Ti: sapphire laser [7]. Nowadays, dispersive mirrors have become the key devices for controlling ultrafast laser systems.

In the course of this development, the output power and beam quality requirements continuously increased; dispersive mirrors with high reflection efficiency and very accurate negative broadband GDD are needed. Modern dispersive mirrors are designed with more than a hundred layers to satisfy the complex requirements of dispersion control in advanced laser systems. For optical coatings with complex structures, different optical monitoring strategies have been applied to different coating types [8,9]. Recent research has shown an error self-compensation effect in direct optical monitoring, which is positive in most cases. Typical beneficial mechanisms are based on compensating for the deviation in the optical thickness by modulating the physical thickness of the current layer [10,11]. However, in the case of the GDD properties of the dispersive mirrors, this compensation effect may be counterproductive. Because the target value for conventional optical monitoring is the transmittance or reflectance data, the compensation process adjusts the optical thicknesses according to the target spectrum rather than the target GDD values [12]. Therefore, complex dispersive mirrors are often fabricated using time monitoring

techniques or quartz crystal monitoring techniques. This approach is ineffective because multiple iterations are required to obtain a stable set of deposition parameters to achieve an accurate GDD [13,14]. In addition, this method relies heavily on the stability of the deposition process; hence, the successful fabrication of complex dispersive mirrors cannot be achieved without advanced and expensive sputtering deposition equipment [15]. The Laser Zentrum Hannover presented a fiber based in-situ Fourier transform GDD measurement system [16] for the optical coating process. This monitoring method provides a new perspective for fabricating optical thin films with good GDD properties. However, to the best of our knowledge, there is no research revealing the error self-compensation mechanism of in-situ GDD monitoring, and comparing the fabrication of dispersive mirrors under the conditions of GDD monitoring, broadband optical monitoring, and time monitoring.

Here, we establish a computational manufacturing program based on GDD monitoring and demonstrate the results of dispersive mirrors in three monitoring strategies: GDD monitoring, broadband optical monitoring, and time monitoring. We demonstrate the mechanism of in-situ direct GDD monitoring for the first time. Section 2 describes a computational manufacturing program for GDD monitoring, and Section 3 describes the computational manufacturing of dispersive mirrors under three monitoring strategies. A discussion of the GDD monitoring mechanism is presented in Section 4. Finally, conclusions are presented in Section 5.

2. Computational manufacturing program of GDD monitoring

Virtual coating programs incorporating modern deposition processes and monitoring strategies are important tools for investigating the preproduction of optical coatings. A virtual coating program built using mathematical methods can rapidly demonstrate the complete coating process. The virtual coating program allows the rapid generation of possible fabrication results and provides a constructive solution for coating designers. Broadband optical monitoring simulators are widely used in practice [17]. In order to expand horizons in the field of coating technology, we developed a GDD monitoring simulator for the deposition processes of multilayer optical coatings, characterized by replacing intensity measurements with phase determination. In this paper, the GDD monitoring simulator is based on the in-situ GDD measurement system in [16]. The idea is the in-situ determination of GDD directly on moving substrates by combining the IBS deposition chamber with a Michelson interferometer. This is achieved by a fiber based in-situ short time Fourier transform measurement device that makes GDD precision comparable to common ex-situ systems.

Let us describe the main algorithmic features of this simulator.

- Let $d_1^{theor}, \ldots, d_m^{theor}$ be the physical thickness of the coating layer, where m is the total number of coating layers. The substrate and thin film materials parameters were determined, and the Cauchy formula was employed to express the dispersion of their refractive indices. The simulator can generate a theoretical GDD curve for each layer based on these parameters.

- The deposition rate of the material is set to v. However, the deposition rate of optical thin film materials is unstable, and we assume that the dependence of the deposition rate on time can be represented by a stationary random process. Hence, v^{rms} is the root mean square fluctuation of the deposition rate with time, and t^{corr} is the correlation time.

- Set j as the current monitoring layer, and the theoretical physics of the current layer is denoted as d_j^{theor}, $j \le m$.

- Let us denote $d_1^{actual}, \ldots, d_{j-1}^{actual}$ as the actual thicknesses of the already deposited layers, where the actual thickness of the *ith* layer is denoted as d_i^{actual}, $1 \le i \le j$. Denote $\delta d_i^{measure}$

as the thickness errors of the *ith* layer caused by monitoring, and the $\delta d_i^{shutter}$ means the thickness error caused by shutter delay. The actual thickness of the *ith* layer can be represented as

$$d_i^{actual} = d_i^{theor} + \delta d_i^{measure} + \delta d_i^{shutter} \tag{1}$$

- The sources of the deposition thickness deviations are multifactorial. Computational manufacturing are valuable only if the error factors are correctly simulated. We denote the mean shutter delay time is $t^{shutter}$, and the shutter delay RMS is $t_{rms}^{shutter}$; The "actual" thickness of the deposition layer $d^{actual}(t_s)$ known to the simulator is calculated from the relation $d^{actual}(t_s) = d^{actual}(t_{s-1}) + v_s(t_s - t_{s-1})$ (s is the index of the deposition time instance). v_s is the time-dependent fluctuating deposition rate generated by the simulator, in which $v_s = v + \delta v^{rms}(t_s)$. This simulator monitoring target is the GDD of coatings. Hence, we assume $GDD^{measure}$ is the real measurement value, and then introduce the error factor measured in the real experiment into the real measurement model of the simulator, including I. random test signal noise $\delta GDD_{random}^{measure}(\lambda, t_s)$ (uncorrelated with respect to λ error with dispersion $\sigma_{random}^{measure}$); II. Systematic error $\delta GDD_{systematic}^{measure}$.

- These data form the basis for calculating the actual $GDD(d_1^{actual}, \ldots, d_{j-1}^{actual}, d^{actual}(t_s), \lambda)$ values at each wavelength λ of the multilayer coating. Consequently, the expression for the real measurement value $GDD^{measure}(d_1^{actual}, \ldots, d_{j-1}^{actual}, d^{actual}(t_s), \lambda, t_s)$ at time t_s takes the following form:

$$GDD^{measure}(d_1^{actual}, \ldots, d_{j-1}^{actual}, d^{actual}(t_s), \lambda, t_s) = GDD$$
$$(d_1^{actual}, \ldots, d_{j-1}^{actual}, d^{actual}(t_s), \lambda) + \delta GDD_{random}^{measure}(\lambda, t_s) + \delta GDD_{systematic}^{measure} \tag{2}$$

The process simulation flow of GDD monitoring is as follows:

a) The designer provides thin film materials, substrate material, and multilayer design data, from which the simulator generates the theoretical GDD curves for each layer.

b) Then, the thin film begins to deposit, and the thickness of the thin film increases with time, where the deposition rate is v_s;

c) The simulator collects the GDD data in real time with a time interval τ, and inverts the thickness of the deposited thin film $d^{estimate}(t_s)$ accordingly. The following formula shows the thickness of the deposited layer at a given time.

$$d^{estimate}(t_s) = \min_d \sum_\lambda$$
$$[GDD(d_1^{estimate}, \ldots d_{j-1}^{estimate}, d, \lambda) - GDD^{measure}(d_1^{actual}, \ldots d_{j-1}^{actual}, d^{actual}(t_s), \lambda, t_s)]^2 \tag{3}$$

d) The deposition of the *jth* layer is terminated when the minimum of the discrepancy function

$$F_j(d) = \min_d \sum_\lambda$$
$$[GDD(d_1^{theor}, \ldots d_{j-1}^{theor}, d^{theor}) - GDD^{Terminate}(d_1^{actual}, \ldots d_{j-1}^{actual}, d^{prediction})]^2 \tag{4}$$

where $GDD^{Terminate}$ denotes the termination curve in the *jth* layer and $d^{prediction}$ denotes the predicted coating stop thickness of the *jth* layer. The prediction of the deposition thickness of the *jth* layer is calculated using the target curve, and the coating of this layer is terminated when the inverse *jth* layer thickness approximates the predicted thickness.

e) If $j < m$, then transition to b) takes place and starts the deposition of the next layer; if $j = m$, the simulator is terminated.

3. Computational manufacturing of dispersive mirrors with different monitoring strategies

This section presents the computational manufacturing of two typical dispersive mirrors for different monitoring simulators. Before conducting the computational manufacturing, it was necessary to provide a feasible design. We present two types of dispersive mirror designs that can compensate for the GDD depicted in Fig. 1 using violet crosses. The substrate was 7980 glass; the layer materials were Ta_2O_5 and SiO_2. The refractive index wavelength dependencies of both the layer materials and substrates are specified by the Cauchy formula $n(\lambda) = A_0 + A_1(\lambda_0/\lambda)^2 + A_2(\lambda_0/\lambda)^4$ with the coefficients presented in Table 1.
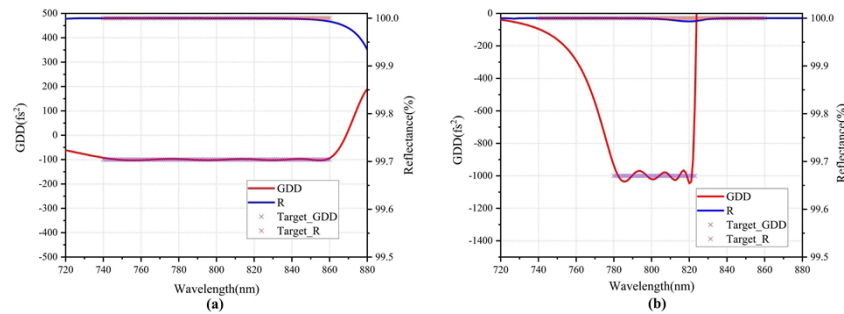
Fig. 1. LDM design(a) and HDM design(b), Reflectance (blue curve), target reflectance (red crosses), GDD (red curve) and target GDD (violet crosses)

Table 1. Cauchy formula coefficients for the substrate and layer materials

Material	A_0	A_1	A_2
Ta_2O_5	2.1050	2.03537×10^{-2}	1.32433×10^{-3}
SiO_2	1.4761	1.50488×10^{-3}	4.30515×10^{-4}
Glass 7980	1.4616	4.36247×10^{-3}	0

We achieved the design with GDD and reflectance, as shown in Fig. 1, using the gradual evolution technique [18] and the OptiLayer software [19]. The level of GDD at 800 nm for the low-dispersion mirror (LDM) in Fig. 1(a) corresponds to $-100fs^2$, and the level of GDD at 800 nm for the high-dispersive mirror (HDM) in Fig. 1(b) corresponds to $-1000fs^2$. The target is indicated by the cross in the illustration.

Delays in the LDM are primarily controlled by the penetration depth effect [20], as shown in Fig. 2(a), which depicts the LDM design structure. The phase delay is achieved by modulating the layer thicknesses close to the incident medium, which allows wavelengths in different frequency domains to penetrate different depths. The regular layer structure near the substrate side ensured a high reflection efficiency at 800 nm. The sensitivity of each LDM layer is shown in Fig. 2(b). The layer sensitivity was calculated based on the deviation of the simulated spectral and GDD features from the theoretical features generated by the layer thickness errors.

For the HDM, the delays are mainly affected by both the penetration depth and the Gires-Tournois interferometer effects [21], as shown in Fig. 3(a). Increasing the number of modulation layers and adding Gires-Tournois cavities to obtain high GDD modulation extends the dwell time of the wavelength in the coatings. However, the layer sensitivity increased owing to the cavity structure.

We describe three monitoring environments for the simulated computational manufacturing after detailing the specifications of the dispersive mirror design. The first is the in-situ GDD
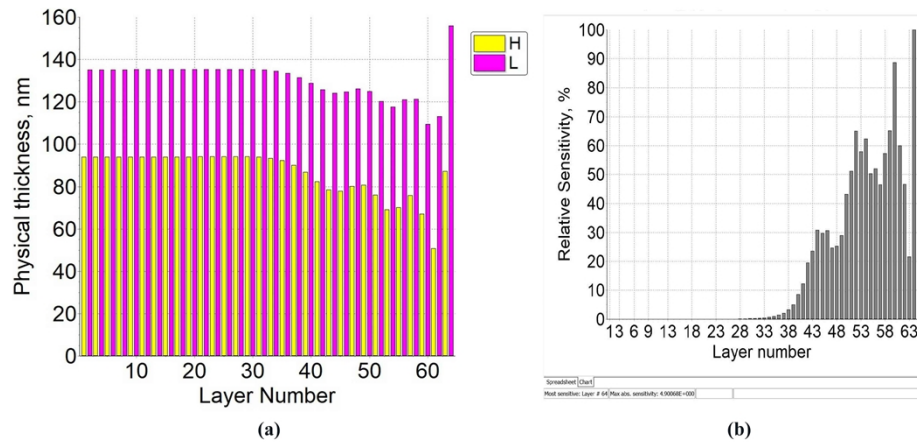
Fig. 2. Optical layer thicknesses of 64-layers LDM design(a) Layer sensitivity of LDM design(b)
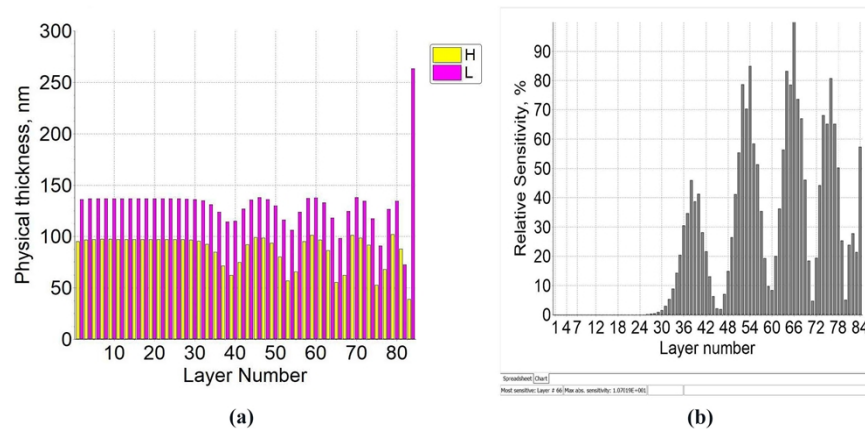
Fig. 3. Optical layer thicknesses of 84-layers HDM design(a) Layer sensitivity of HDM design(b)

monitoring discussed in Section 2. The second is the in-situ broadband monitoring in the OptiLayer software, which was introduced in [19]. The third type is time monitoring, in which the level of thickness error is the same for all layers. These errors were normally distributed, and the mathematical expectation and standard deviation were set to 1%. Table 2 displays the detailed parameters set in the simulation calculation of the deposition simulation under various monitoring conditions.

Virtual deposition simulations were performed based on these parameters. Figure 4 depicts the simulation results of the virtual LDM deposition in the three monitoring environments. In Fig. 4, the blue and red curves represent the results of a single run of GDD monitoring and broadband monitoring of computational manufacturing, respectively. For time monitoring, 1000 run simulations were performed, and an orange corridor was displayed that corresponded to the deviations of the GDD characteristics from their mathematical expectations. Note that the width of the corridor depends on the probability that the selected characteristic value falls within the corridor, which we set to 80%. We took the findings of one of the time monitoring runs and plotted them as orange curve. The three simulation results show that the GDD characteristics

Table 2. Monitoring parameters of computational manufacturing

Parameters	Broadband monitoring	GDD monitoring	Time monitoring
Deposition rate (Ta_2O_5)	0.24 nm/s	0.24 nm/s	-
Deposition rate (SiO_2)	0.18 nm/s	0.18 nm/s	-
Deposition rate RMS (Ta_2O_5)	0.012 nm/s	0.012 nm/s	-
Deposition rate RMS (SiO_2)	0.018 nm/s	0.018 nm/s	-
Correlation time	3s	3s	-
Monitoring wavelength	500~1050	750~850	-
Wavelength points	551	101	-
Mean shutter delay	0.5 s	0.5 s	-
Shutter delay RMS	0.5 s	0.5 s	-
Scan interval	3 s	3 s	-
Monitoring random error	3%	3%	-
Measure mode	transmittance	GDD	time
Physical thickness error (Relative RMS)	-	-	1%

for both GDD and broadband monitoring fall inside the time monitoring corridor, indicating that GDD monitoring techniques are more suitable for LDM fabrication. The computational manufacturing results correlated well with the theoretical curve in the GDD monitoring range (750–850 nm).
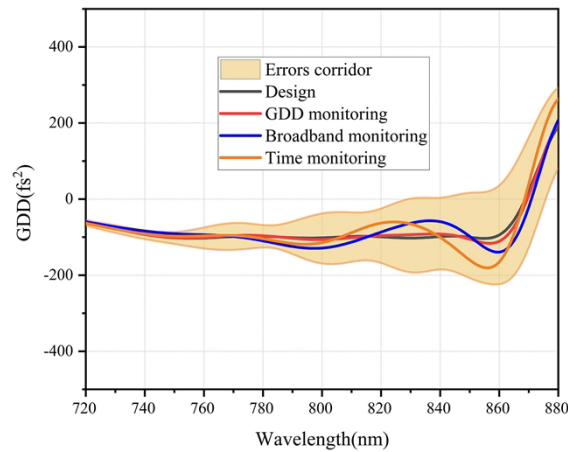
Fig. 4. The theoretical GDD (black curve), simulated GDD (GDD monitoring—red curve, broadband monitoring—blue curve, and time monitoring—orange curve) and a corridor of time monitoring GDD errors (orange area) for the LDM simulation results

The distribution of layer thickness errors during several monitoring simulations is shown in Fig. 5. The layer thickness errors in the time monitoring were smaller than those in the GDD and broadband monitoring, especially in the last few layers. Although the relative thickness errors of the layers were high during GDD monitoring, the final results deviated the least from the theoretical design. It is plausible to assume that, as with the error self-compensation effect of broadband monitoring for spectral characteristics [9], the error self-compensation effect exists when GDD monitoring targets GDD characteristics.

The HDM computational manufacturing were conducted in the same monitoring environment, and the simulated results are shown in Fig. 6. The simulation findings of broadband monitoring
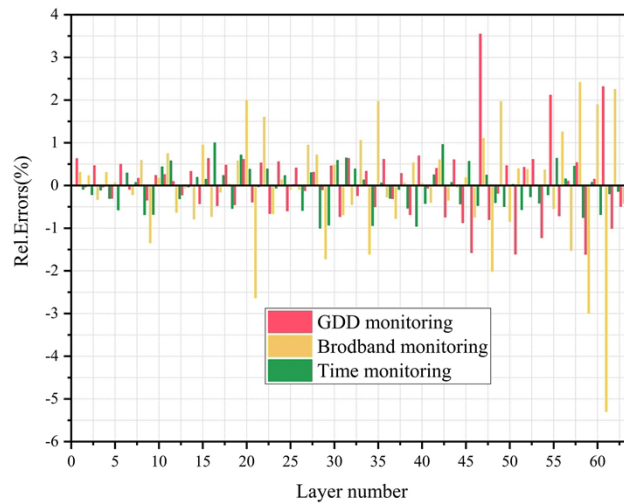
Fig. 5. Relative errors in 64-layers thicknesses of deposition simulations

and time monitoring in the concerned wavelength range (780–820 nm) deviate significantly from the design curve. In contrast, the results of GDD monitoring show that the GDD deviates within an acceptable range, with deviations less than 30% of the target value.
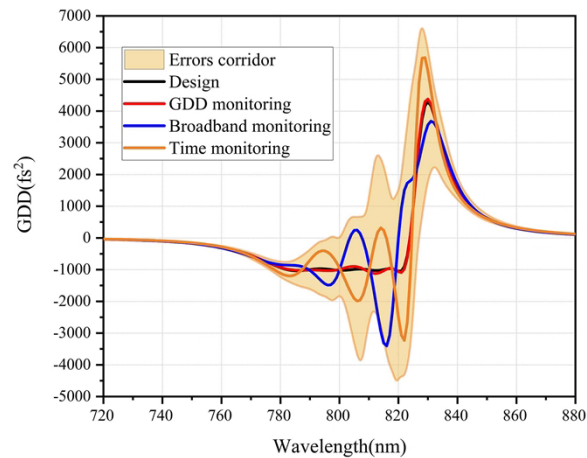
Fig. 6. The theoretical GDD (black curve), simulated GDD (GDD monitoring—red curve, broadband monitoring—blue curve, time monitoring—orange curve), and a corridor of time monitoring GDD errors (orange area) for the HDM simulation results

The layer thickness error distributions of HDM different monitoring simulations are shown in Fig. 7. The relative layer thickness errors for both GDD and broadband monitoring were higher than the relative thickness errors for time monitoring. With an increase in the number of deposited layers, the thickness error increases owing to the cumulative effect of the thickness errors. Although the relative thickness errors of the HDM and LDM are similar, the HDM is more sensitive to the thickness error, as demonstrated in Fig. 2(b), resulting in the simulation of the computational manufacturing with broadband monitoring deviating greatly from the theoretical design. This implies that precisely fabricating a high reflection mirror with a high GDD via time monitoring or broadband monitoring is challenging. Consequently, GDD monitoring

demonstrated distinct advantages in the fabrication of dispersive mirrors. This benefit stems from our assumption of error self-compensation in GDD monitoring. According to the results of the two GDD monitoring computational manufacturing, the relative thickness errors of the layers are larger than the time monitoring errors, partly because of the cumulative effect of direct monitoring thickness errors but primarily because of the process of re-optimization of the target thickness during the termination course.
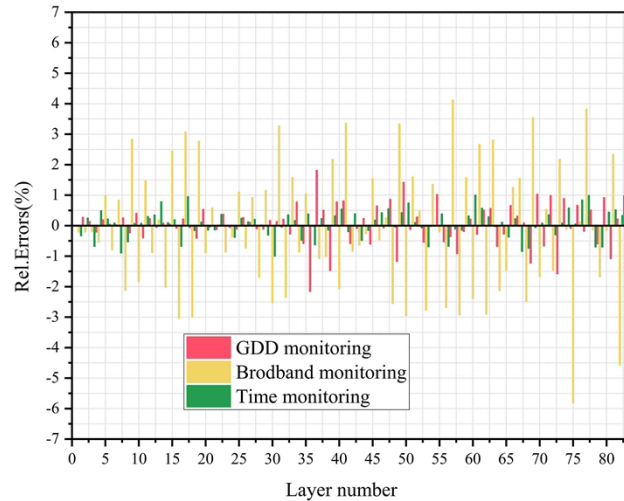
Fig. 7. Relative errors in 84-layers thicknesses of deposition simulations

In the above simulation environment, GDD and broadband monitoring random error and spectral resolution are equal. In practice, the measurement error levels of the GDD measurement system based on Fourier transform is higher than that of the broadband monitoring system [22]. In Fig. 8, we present the GDD simulation curves obtained by varying the GDD monitoring random
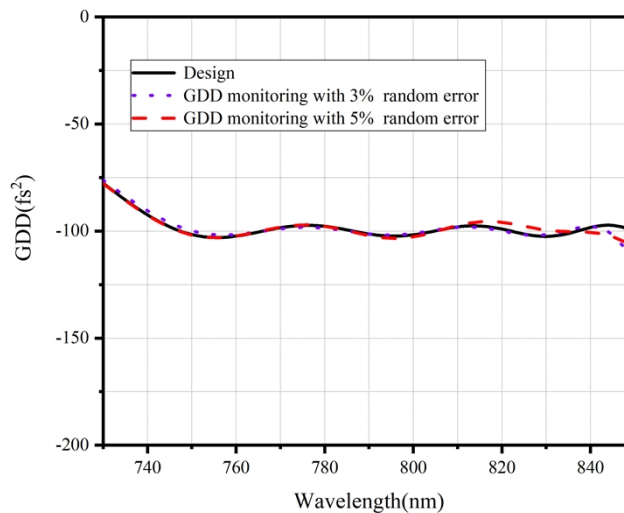
Fig. 8. The theoretical GDD (black curve), simulated GDD (GDD monitoring with 3% random error —dot curve, GDD monitoring with 5% random error—dashed curve) for the LDM

error and the wavelength points. First, one can see that when the GDD monitoring random error increases from 3% to 5%, there is no significant deviation in the results of the simulated GDD curve. Second, one can conclude that a reasonable increase in the GDD monitoring random error does not significantly affect the results of computational manufacturing dispersion mirrors.

4. Discussion on the error self-compensation mechanism of GDD monitoring

The simulated results in Section 3 demonstrate the excellent performance of GDD monitoring in manufacturing dispersive mirrors and reveal the possible error self-compensation effect in the process. It was already indicated that the error self-compensation effect in the monitoring process is related to the thickness error correlation caused by direct monitoring [23].

An effective approach to demonstrate the existence of the error self-compensation effect is to compare the manufacturing results under correlated and uncorrelated thickness error conditions [24]. The computational manufacturing process introduces various random factors that cause thickness errors. Therefore, the simulated results of the thickness error correlation require statistical analysis. Therefore, to further illustrate the error self-compensation effect, we built a simplified GDD monitoring simulation tool that can be used to generate thousands of simulations in real time.

The process of the simplified simulator is as follows:

a) In the first deposited layer, the actual thickness of the first layer is $d_1 = d_1^{theor} + v_1$ due to the shutter delay, where v_1 follows a normal distribution with a random error $v_1 \sim N(\mu_1, \sigma_1^2)$;

b) When depositing the *jth* layer, the target thickness of the layer is determined based on the minimum merit function.

$$d_i^{target} = argmin \sum_\lambda (GDD(\lambda, d_1^{theor}, d_1^{theor}, \dots, d_i^{theor}) - GDD(\lambda, d_1^{actual}, d_1^{actual}, \dots, d_i^{target}))^2$$

(5)

c) Redefine $d_i^{act} = d_i^{target} + v_i$, where v_i is a normally distributed random error.

d) If $j < m$, then go to step b.

e) After all layers are deposited, the thickness error of the thin film is $\delta d_i = d_i^{act} - d_i^{theor}$

In the simplified simulator, v_i is a random error caused by various factors. The deposition rate v_s follows a normal distribution with a random error $v_i \sim N(\mu_v, \sigma_v^2)$, and the shutter delay $t^{shutter}$ follows a normal distribution with a random error $t_{delay} \sim N(\mu_t, \sigma_t^2)$. In the simplified simulator, we ignore the GDD measurement error. Then, the random error v_i is the deposition residual due to the shutter delay, and its statistical parameters are calculated as

$$\mu_i = E(v_i t_{delay}) = \mu_v \mu_t,$$ (6)

$$\sigma_i^2 = D(v_i t_{delay})$$
$$= E(v_i^2)E(t_{delay}^2) - E(v_i)^2 E(t_{delay})^2$$
$$= (\mu_v^2 + \sigma_v^2)(\mu_t^2 + \sigma_t^2) - \mu_v^2 \mu_t^2$$
$$= \mu_v^2 \sigma_t^2 + \mu_t^2 \sigma_v^2 + \sigma_v^2 \sigma_t^2.$$

(7)

In the simplified simulator, we use a nonlinear programming approach that constrains the thickness range to 0.97–1.03 D to find the minimum value of the merit function.

A statistical analysis of the results of the simplified simulator monitoring the two types of dispersive mirrors is shown in Fig. 9. Each design was simulated 1000 times to provide a sufficient

sample of data. As shown in Fig. 4, the orange area in Fig. 9 represents the corridor width with an 80% probability for 1000 simulations. The red area depicts the results of 1000 runs of the simplified GDD simulator. The corridor width is determined by the 90% probability that the selected characteristic values fall within the corridor. The results of 10 simulations were chosen at random from 1000 runs of the simplified GDD simulator and are represented as black curves. The time monitoring simulation was considered a simulation with uncorrelated thickness errors. The errors in layer thicknesses were normally distributed with zero mathematical expectation, but the standard deviation was set to 1% for all layers. GDD simulation monitoring can be regarded as a correlated thickness error simulation with a root mean square error level of approximately 3%. The statistical analysis results show that the corridor width of the GDD monitoring simulator is significantly smaller than that of time monitoring. This implies that the uncorrelated thickness errors destroy the dispersive mirror's GDD properties. There is also an error self-compensation effect in the GDD monitoring process. This also implies that manufacturing dispersive mirrors is more deterministic when GDD monitoring is used.
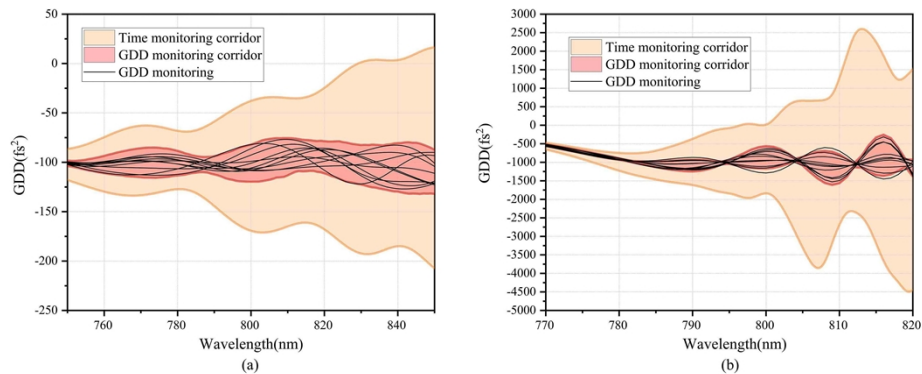
Fig. 9. Statistical simulation results of 1000 time monitoring simulations and GDD monitoring simulations, simulation results with LDM (a) and HDM (b), a corridor of 80% probability for 1000 time simulations with the same 1% levels for all coating layers (orange area), a corridor of 90% probability for 1000 time simulations with GDD monitoring (red area), and the results of 10 runs were randomly selected from 1000 GDD monitoring simulations (black curve).

The existence of an error self-compensation effect in the GDD monitoring process is predictable. There is an error self-compensation effect in the broadband monitoring process, and the mathematical mechanism of the error self-compensation effect in broadband monitoring was investigated in [25]. The results show that when the monitoring and design merit functions have the same variables, the two evaluation functions are matched, and the thickness errors can compensate for the spectral variation. Essentially, the flow of the GDD monitoring simulation calculation program is similar to that of the broadband monitoring simulator [26]. The difference is that all target variables in the coating process are GDD coefficients and are no longer T/R spectral coefficients.

In GDD monitoring, the design optimization function is shown as

$$MF = \sum_{\lambda} \left(\frac{GDD - GDD_0}{\Delta} \right)^2 \tag{8}$$

The merit function in the GDD monitoring process is expressed as

$$F_j(d) = \min_d \sum_\lambda$$

$$[GDD(d_1^{theor}, \ldots d_{j-1}^{theor}, d^{theor}) - GDD^{Terminate}(d_1^{actual}, \ldots d_{j-1}^{actual}, d^{prediction})]^2 \tag{9}$$

Predicting the current layer stop thickness in GDD monitoring is a re-optimization process; therefore, the variation in GDD can be compensated by modulating the deposited layer thickness. Therefore, there is an error self-compensation effect in the GDD monitoring.

In addition, GDD monitoring has a significant advantage in that its inversion error of GDD monitoring is lower than that of broadband monitoring. In GDD monitoring, analogous to the method used in the analysis of broadband monitoring in [27], the inversion error function can be written as

$$\delta d_j = \sum_{i=1}^{j-1} \alpha_j^i \delta d_i + \beta_j, \tag{10}$$

Equation (10) represents the error between the actual and determinate thickness of the *jth* layer. Where β_j denotes the thickness error caused by the systematic error in the monitoring data of the *jth* layer as follows:

$$\beta_j = \frac{\sum\limits_{\{\lambda\}} \left(-\frac{\partial GDD^j}{\partial d_j} \, \delta GDD_{meas}(\lambda) \right)}{\sum\limits_{\{\lambda\}} \left(\frac{\partial GDD^j}{\partial d_j} \right)^2} \tag{11}$$

β_j in Eq. (11) is influenced by the first-order partial derivative. The GDD of the dispersive mirror is more sensitive to the thickness than the transmittance coefficient and is expressed as follows:

$$\frac{\sigma_{GDD}}{\sum\limits_{\{\lambda\}} \left| \frac{\partial GDD}{\partial d} \right|} < \frac{\sigma_T}{\sum\limits_{\{\lambda\}} \left| \frac{\partial T}{\partial d} \right|}. \tag{12}$$

where σ_{GDD} and σ_T denote the standard deviations of the random errors during GDD and broadband monitoring, respectively. Therefore, under the same monitoring wavelength, the inversion thickness error caused by the GDD monitoring data was smaller than that of broadband monitoring.

The first term on the right side of Eq. (10) represents the thickness error resulting from the random thickness error due to the accumulation of test errors during monitoring. Where α_j^i is expressed as follows:

$$\alpha_j^i = \frac{-\sum\limits_{\{\lambda\}} \left(\frac{\partial GDD^j}{\partial d_j} \frac{\partial GDD^j}{\partial d_i} \right)}{\sum\limits_{\{\lambda\}} \left(\frac{\partial GDD^j}{\partial d_j} \right)^2} \tag{13}$$

Although the inversion accuracy of GDD monitoring was improved, Eq. (13) cannot be optimized to zero, and there is still an accumulated error in the inversion thickness. Because the inversion accuracy of GDD monitoring is higher than that of broad-spectrum monitoring, the error accumulation effect of GDD monitoring is weaker than that of broadband monitoring. Thus, with the same level of measurement errors, one should expect the inversion error level of the GDD monitoring approach to be smaller. This finding illustrates that GDD monitoring can be used as a new technique to achieve high-precision control of coating thickness. If suitable monitoring algorithms are developed, GDD monitoring can be used to fabricate diverse optical coatings.

5. Conclusion and outlook

This work presents an in-situ GDD monitoring simulator that can run a computational manufacturing and provide relevant data variables in a couple of minutes. The performances of GDD monitoring, broadband monitoring, and time monitoring in dispersive mirror fabrication simulations were compared. The results revealed the particular advantages of GDD monitoring in dispersive mirror fabrication simulations.

The simulation results of the GDD monitoring, broadband monitoring, and time monitoring simulations for manufacturing dispersive mirrors showed that the fabrication GDD curves deviated the least from the theoretical values. However, the level of the relative thickness errors of GDD monitoring was not the smallest. In Section 4, statistical analysis of many simulations demonstrates the error self-compensation effect in GDD monitoring. The error self-compensation mechanism for GDD targets is derived from predicting the current layer stop thickness in GDD monitoring as a re-optimization process. The absence of error self-compensation effect in the time monitoring process of fabricating of dispersive mirrors is due to the non-correlation of thickness errors, and the inability of broadband monitoring to compensate for GDD targets is due to the inconsistency between the variables of the design merit function and the monitoring merit function.

Finally, GDD monitoring is particularly sensitive to optical thickness variations, allowing for a more precise layer thickness inversion. It may become a possible new control technology for manufacturing different types of optical coatings. We will do further research in the future.

Disclosures. The authors declare no conflicts of interest.

Data availability. The data underlying the results presented in this paper can be obtained from the authors upon reasonable request.

References

1. T. Udem, R. Holzwarth, and T. W. Hänsch, "Optical frequency metrology," Nature **416**(6877), 233–237 (2002).
2. S. H. Chung and E. Mazur, "Surgical applications of femtosecond lasers," J. Biophotonics **2**(10), 557–572 (2009).
3. R. Szipöcs, K. Ferencz, C. Spielmann, and F. Krausz, "Chirped multilayer coatings for broadband dispersion control in femtosecond lasers," Opt. Lett. **19**(3), 201–203 (1994).
4. H. A. Macleod, *Thin-Film Optical Filters* (4th ed). (Taylor & Francis, 2010).
5. A. Wirth, M. T. Hassan, I. Grguras, J. Gagnon, A. Moulet, T. T. Luu, S. Pabst, R. Santra, Z. A. Alahmed, A. M. Azzeer, V. S. Yakovlev, V. Pervak, F. Krausz, and E. Goulielmakis, "Synthesized light transients," Science **334**(6053), 195–200 (2011).
6. V. Pervak, O. Razskazovskaya, I. B. Angelov, K. L. Vodopyanov, and M. Trubetskov, "Dispersive mirror technology for ultrafast lasers in the range 220–4500 nm," Adv. Opt. Technol. **3**(1), 55–63 (2014).
7. V. Pervak, A. V. Tikhonravov, M. K. Trubetskov, S. Naumov, F. Krausz, and A. Apolonski, "1.5-octave chirped mirror for pulse compression down to sub-3 fs," Appl. Phys. B **87**(1), 5–12 (2007).
8. A. V. Tikhonravov and M. K. Trubetskov, "Automated design and sensitivity analysis of wavelength-division multiplexing filters," Appl. Opt. **41**(16), 3176–3182 (2002).
9. V. Zhupanov, I. Kozlov, V. Fedoseev, P. Konotopov, M. Trubetskov, and A. Tikhonravov, "Production of Brewster-angle thin film polarizers using ZrO₂ /SiO₂ pair of materials," Appl. Opt. **56**(4), C30–C34 (2017).
10. A. V. Tikhonravov, M. K. Trubetskov, and T. V. Amotchkina, "Investigation of the error self-compensation effect associated with broadband optical monitoring," Appl. Opt. **50**(9), C111–C116 (2011).
11. A. V. Tikhonravov, I. V. Kochikov, and A. G. Yagola, "Investigation of the error self-compensation effect associated with direct broad band monitoring of coating production," Opt. Express **26**(19), 24964–24972 (2018).
12. T. Willemsen, S. Schlichting, T. Kellermann, M. Jupé, H. Ehlers, U. Morgner, and D. Ristau, "Precise fabrication of ultra violet dielectric dispersion compensating mirrors," Proc. SPIE **9627**, 96271U (2015).
13. Y. Chen, D. Hahner, M. Trubetskov, and V. Pervak, "Suppression of group delay dispersion oscillations of highly dispersive mirrors by non-uniformity and post-deposition treatment," Opt. Laser Technol. **142**, 107192 (2021).
14. M. Trubetskov, T. Amotchkina, A. Tikhonravov, and V. Pervak, "Reverse engineering of multilayer coatings for ultrafast laser applications," Appl. Opt. **53**(4), A114–A120 (2014).
15. Y. Chen, D. Hahner, M. Trubetskov, W. Sakiew, K. Starke, and V. Pervak, "Comparison of magnetron sputtering and ion beam sputtering on dispersive mirrors," Appl. Phys. B **126**(5), 82 (2020).

16. S. Schlichting, T. Willemsen, H. Ehlers, U. Morgner, and D. Rista, "Fourier-transform spectral interferometry for in situ group delay dispersion monitoring of thin film coating processes," Opt. Express **24**(20), 22516–22527 (2016).

17. A. V. Tikhonravov and M. K. Trubetskov, "Computational manufacturing as a bridge between design and production," Appl. Opt. **44**(32), 6877–6884 (2005).

18. A. V. Tikhonravov, M. K. Trubetskov, and G. W. DeBell, "Optical coating design approaches based on the needle optimization technique," Appl. Opt. **46**(5), 704–710 (2007).

19. A. V. Tikhonravov and M. K. Trubetskov, OptiLayer Thin Film Software, http://www.optilayer.com

20. F. X. Kärtner, N. Matuschek, T. Schibli, and U. Keller, "Design and fabrication of double-chirped mirrors," Opt. Lett. **22**(11), 831 (1997).

21. B. Golubovic, R. R. Austin, M. K. Steiner-Shepard, M. K. Reed, S. A. Diddams, D. J. Jones, and A. G. Van Engen, "Double Gires-Tournois interferometer negative-dispersion mirrors for use in tunable mode-locked lasers," Opt. Lett. **25**(4), 275–277 (2000).

22. T. V. Amotchkina, A. V. Tikhonravov, M. K. Trubetskov, D. Grupe, A. Apolonski, and V. Pervak, "Measurement of group delay of dispersive mirrors with white-light interferometer," Appl. Opt. **48**(5), 949–956 (2009).

23. A. V. Tikhonravov, I. V. Kochikov, S. V. Sharapova, and A. G. Yagola, "Optical monitoring of coating production: correlation of errors and errors self-compensation," Proc. SPIE **11872**, 118720Q (2021).

24. X. Ji, J. Zhang, H. Jiao, X. Cheng, Z. Wang, I. Kochikov, A. Sharov, and A. Tikhonravov, "Production of ultra-steep dichroic filters with broad band optical monitoring," Opt. Express **30**(13), 22501–22511 (2022).

25. B. T. Sullivan and J. A. Dobrowolski, "Deposition error compensation for optical multilayer coatings. I. Theoretical description," Appl. Opt. **31**(19), 3821–3835 (1992).

26. A. V. Tikhonravov, I. V. Kochikov, and A. G. Yagola, "Mathematical investigation of the error self-compensation mechanism in optical coating technology," Inverse Probl. Sci. Eng. **26**(8), 1214–1229 (2018).

27. A. V. Tikhonravov, M. K. Trubetskov, and T. V. Amotchkina, "Investigation of the effect of accumulation of thickness errors in optical coating production by broadband optical monitoring," Appl. Opt. **45**(27), 7026 (2006).